Cell Reports

Innate Immune Signaling in *Drosophila* Blocks Insulin Signaling by Uncoupling PI(3,4,5)P_3 Production and Akt Activation

Graphical Abstract

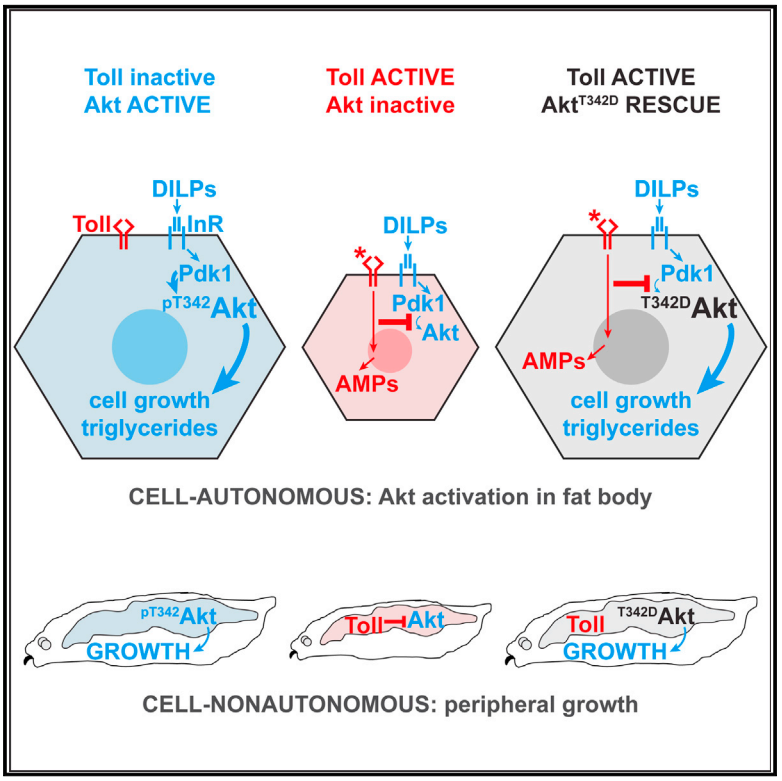

Highlights

- Toll acts cell autonomously to induce insulin resistance in the *Drosophila* fat body
- Fat body Toll signaling reduces growth and triglyceride storage without altering circulating Dilp2 levels
- Toll signaling acts at or downstream of the kinase Pdk1 to reduce Akt phosphorylation
- Mimicking Akt activation loop phosphorylation rescues Toll-dependent phenotypes

Authors

Stephen W. Roth, Moshe D. Bitterman, Morris J. Birnbaum, Michelle L. Bland

Correspondence

mlb2eg@virginia.edu

In Brief

Innate immune signaling through Toll family receptors induces insulin resistance. Roth et al. find that phosphorylation of Akt by Pdk1 is inhibited by Toll signaling in the *Drosophila* larval fat body. Toll-dependent impairments in fat body cell growth, nutrient storage, and peripheral growth are rescued by mimicking Akt activation loop phosphorylation.

Roth et al., 2018, Cell Reports *22*, 2550–2556
March 6, 2018
https://doi.org/10.1016/j.celrep.2018.02.033

CellPress

OPEN ACCESS
CellPress

Cell Reports
Report

Innate Immune Signaling in *Drosophila* Blocks Insulin Signaling by Uncoupling PI(3,4,5)P_3 Production and Akt Activation

Stephen W. Roth,[1] Moshe D. Bitterman,[2] Morris J. Birnbaum,[2,3] and Michelle L. Bland[1,4,*]
[1]Department of Pharmacology, University of Virginia, Charlottesville, VA 22908, USA
[2]Department of Medicine, University of Pennsylvania, Philadelphia, PA 19104, USA
[3]Present address: Internal Medicine Research Unit, Pfizer, Inc., Cambridge, MA 02139, USA
[4]Lead Contact
*Correspondence: mlb2eg@virginia.edu
https://doi.org/10.1016/j.celrep.2018.02.033

SUMMARY

In obese adipose tissue, Toll-like receptor signaling in macrophages leads to insulin resistance in adipocytes. Similarly, Toll signaling in the *Drosophila* larval fat body blocks insulin-dependent growth and nutrient storage. We find that Toll acts cell autonomously to block growth but not PI(3,4,5)P_3 production in fat body cells expressing constitutively active PI3K. Fat body Toll signaling blocks whole-animal growth in *rictor* mutants lacking TORC2 activity, but not in larvae lacking *Pdk1*. Phosphorylation of Akt on the Pdk1 site, Thr342, is significantly reduced by Toll signaling, and expression of mutant Akt^{T342D} rescues cell and animal growth, nutrient storage, and viability in animals with active Toll signaling. Altogether, these data show that innate immune signaling blocks insulin signaling at a more distal level than previously appreciated, and they suggest that manipulations affecting the Pdk1 arm of the pathway may have profound effects on insulin sensitivity in inflamed tissues.

INTRODUCTION

Throughout the animal kingdom, loss-of-function mutations in insulin signaling molecules such as the kinase Akt disrupt cell, organ, and animal growth and derail glucose homeostasis. In humans, insulin resistance and diabetes are rarely due to single-gene mutations. Rather, obesity is a major risk factor for diabetes, and one characteristic of obese adipose tissue is an increased number of macrophages (Weisberg et al., 2003; Xu et al., 2003). Macrophages can account for up to 40% of cells in obese fat, and most monocytes that infiltrate obese fat differentiate into macrophages that express proinflammatory cytokines. Toll-like receptor 4 (TLR4) signaling in these cells drives secretion of cytokines that interfere with insulin signaling in adipocytes (Lackey and Olefsky, 2016). Deletion of *Tlr4* in macrophages and other bone marrow-derived cells or in hepatocytes or adipocytes reduces insulin resistance in high-fat diet-fed mice (Jia et al., 2014; Saberi et al., 2009; Tao et al., 2017), indicating that TLR4 expression is required in immune and metabolic tissues for diet-induced insulin resistance.

How innate immune signaling promotes insulin resistance is unknown. In mammals, inhibition of insulin signaling by cytokine and TLR signaling is associated with serine phosphorylation of insulin receptor substrate (IRS) proteins by kinases such as JNK and IKK (Boura-Halfon and Zick, 2009). Surprisingly, knockin mutations that prevent *Irs1* serine phosphorylation lead to impaired rather than enhanced insulin sensitivity. This calls into question the role of these sites in the mechanism of insulin resistance and suggests that more distal steps of the pathway are subject to regulation (Copps et al., 2010, 2016; Hoehn et al., 2008).

The highly conserved insulin and Toll signaling pathways operate in the same cells of the fat body in the model organism *Drosophila melanogaster*. Insulin signaling in the fat body promotes nutrient storage, fat body cell growth, and whole-animal growth (Arrese and Soulages, 2010; Géminard et al., 2009). In response to infection, Toll signaling in the fat body drives secretion of antimicrobial peptides that kill invading microorganisms (Buchon et al., 2014). In flies, as in mammals, the insulin signaling pathway and innate immune system interact. Infection of adult flies with the bacterial pathogen *Mycobacterium marinum* leads to progressive wasting and reduced Akt phosphorylation (Dionne et al., 2006). Reduced IRS function in adult *chico* mutants improves survival in response to infection (Libert et al., 2008). Activation of Toll signaling in the larval fat body, either genetically or by infection, inhibits insulin signaling and whole-animal growth (DiAngelo et al., 2009). Here, we show that Akt phosphorylation by Pdk1 is strongly inhibited in response to Toll pathway activation in the *Drosophila* larval fat body.

RESULTS

Toll Signaling Blocks Insulin Signaling in a Cell-Autonomous Manner

To identify the point of interaction between fat body Toll and insulin signaling pathways, we carried out genetic epistasis experiments using Akt phosphorylation, cell and animal growth, and triglyceride storage as readouts for insulin signaling. Following insulin receptor (InR) activation, phosphatidylinositol 3-kinase (PI3K) generates PI(3,4,5)P_3, which recruits Pdk1, mTORC2, and Akt to the plasma membrane where Pdk1 and

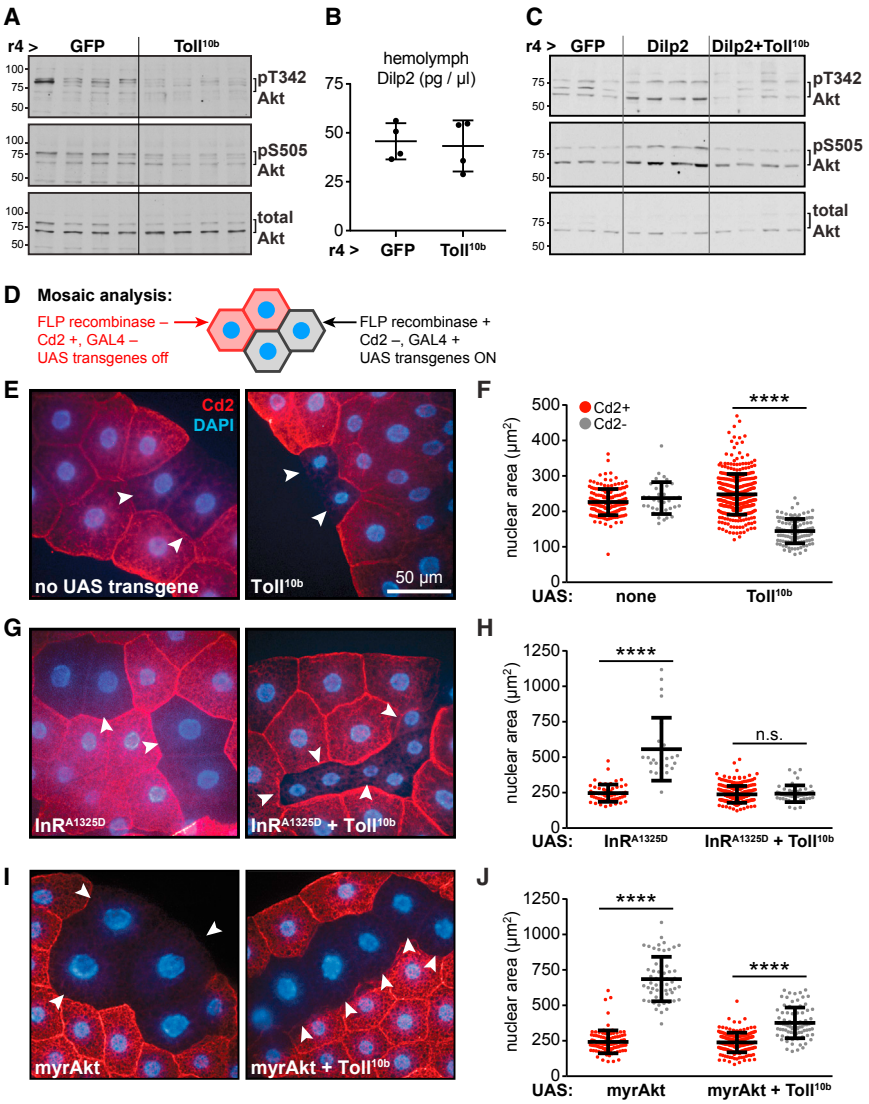

Figure 1. Toll Signaling Blocks Insulin Signaling in a Cell-Autonomous Manner

(A) Western blot analysis of phosphorylated (pT342 and pS505) and total Akt in fat bodies, n = 4/group (gp).

(B) Hemolymph Dilp2 levels in mid-third-instar larvae, n = 4/gp.

(C) Western blot analysis of pT342, pS505, and total Akt in whole larvae, n = 3–4/gp.

(D) Mosaic analysis using the FLP; Act5c > Cd2 > GAL4 system.

(E–J) (E), (G), and (I): micrographs of fat bodies containing WT, $Cd2^+$, $GAL4^-$ cells (red) and transgene-expressing, $Cd2^-$, $GAL4^+$ cells (arrowheads). Nuclei are stained with DAPI (blue). Scale bar, 50 µm. (F), (H), and (J): nuclear area in $Cd2^+$, $GAL4^-$ (red), and $Cd2^-$, $GAL4^+$ (gray) cells. ****$p < 0.0001$ versus $Cd2^+$. UAS-transgenes expressed in $Cd2^-$, $GAL4^+$ cells are as follows: (E and F) left, no transgene ($Cd2^+$, n = 169; $Cd2^-$, n = 36), and right, $Toll^{10b}$ ($Cd2^+$, n = 368; $Cd2^-$, n = 108); (G and H) left, InR^{A1325D} ($Cd2^+$, n = 56; $Cd2^-$, n = 22), and right, InR^{A1325D} + $Toll^{10b}$ ($Cd2^+$, n = 246; $Cd2^-$, n = 45); (I and J) left, myrAkt ($Cd2^+$, n = 100; $Cd2^-$, n = 57), and right, myrAkt + $Toll^{10b}$ ($Cd2^+$, n = 176; $Cd2^-$, n = 81). Data are presented as mean ± SD. See also Table S1 and Figures S1 and S2.

mTORC2 phosphorylate Akt on Thr342 and Ser505 (T308 and S473 in mAkt1), respectively. Expression of constitutively active Toll receptors ($Toll^{10b}$) in larval fat body under control of r4-GAL4 led to reduced Akt S505 phosphorylation in this organ, in agreement with previous findings (Figure 1A) (DiAngelo et al., 2009). Using an antibody that we generated to recognize Akt phosphorylated on T342 (Figure S1A), we found that phosphorylation on this site was also decreased in fat bodies expressing $Toll^{10b}$, while total Akt levels were unchanged (Figure 1A). Larvae expressing GFP or $Toll^{10b}$ in fat body had equivalent hemolymph levels of *Drosophila* insulin-like peptide 2 (Dilp2), an InR ligand secreted by insulin-producing cells in the brain (Figure 1B) (Brogiolo et al., 2001), suggesting that Toll signaling induces insulin resistance rather than insulin insufficiency. To test this, we asked whether Toll signaling could disrupt insulin signaling in animals with elevated Dilp2. Transgenic misexpression of Dilp2 in fat body led to increased Akt phosphorylation in whole larvae, and this was blocked when $Toll^{10b}$ was co-expressed (Figure 1C). Similarly, fat body Toll signaling blocked triglyceride storage in larvae misexpressing Dilp2 in fat body (Figure S2A).

Because fat body Toll signaling blocked Akt activation in animals with normal or elevated Dilp2 levels, we asked whether the Toll pathway acted cell autonomously to induce insulin resistance. We generated mosaic fat bodies containing clones of cells expressing $Toll^{10b}$ alone or with transgenes encoding active insulin signaling pathway components (Figure 1D). Endoreplication in fat body cells leads to tandem increases in nuclear and cell size; we therefore measured nuclear area as a proxy for cell growth (Britton et al., 2002). Nuclear area was equivalent in $GAL4^+$, $Cd2^-$ cells lacking UAS transgenes and their wild-type (WT) $GAL4^-$, $Cd2^+$ neighbors. In contrast, GAL4+, Cd2-cells expressing $Toll^{10b}$ were small with significantly smaller nuclei than WT cells (Figures 1E and 1F). Expression of constitutively active InR^{A1325D} drove an increase in nuclear area, and this was blocked by co-expression of $Toll^{10b}$ (Figures 1G and 1H). We noted that Toll signaling reduced whole-cell area in cells expressing InR^{A1325D}, perhaps by blocking nutrient storage. Indeed, triglyceride levels were reduced when $Toll^{10b}$ was expressed alone or with InR^{A1325D} (Figure S2B).

Expression of $Toll^{10b}$ throughout the fat body impairs whole-animal growth, and this is rescued by co-expression of myristoylated Akt (myrAkt), a constitutively active Akt transgene (DiAngelo et al., 2009). Fat body cells expressing myrAkt were large with large nuclei. In contrast to results with InR^{A1325D}, cells

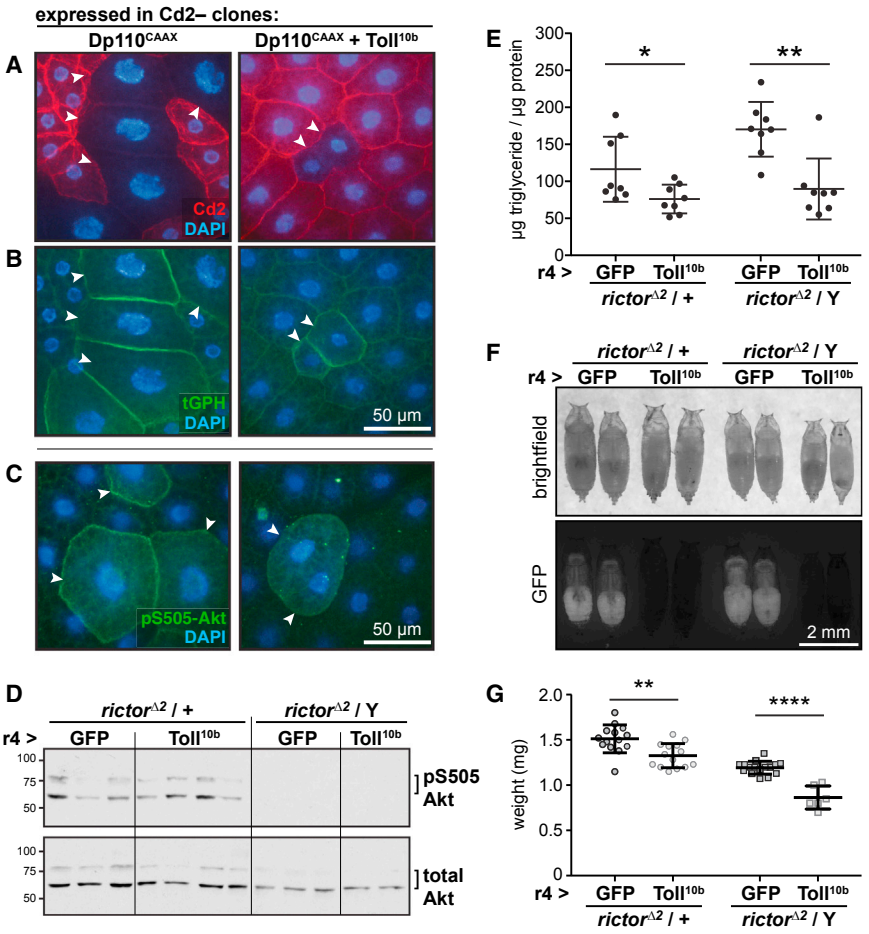

Figure 2. Toll Signaling Acts Independently of TORC2 to Block Insulin Signaling

(A–C) Micrographs of fat bodies containing $Cd2^+$ WT cells (red, nuclear area, left: 240.0 ± 80.2 μm^2, n = 101; right: 245.6 ± 99.0 μm^2, n = 118) and $Cd2^-$, $GAL4^+$ cells (arrowheads) expressing $Dp110^{CAAX}$ (left, nuclear area: 648.7 ± 193.0 μm^2, n = 31, $p < 0.0001$ versus $Cd2^+$) or $Dp110^{CAAX}$ + $Toll^{10b}$ (right, nuclear area: 334.3 ± 119.5 μm^2, n = 33, $p < 0.0001$ versus $Cd2^+$). Nuclei are stained with DAPI (blue). Scale bars, 50 μm. (A) Immunocytochemistry for Cd2 (red). (B) Plasma membrane localization of the ubiquitously expressed $PI(3,4,5)P_3$ reporter tGPH (green) in cells expressing $Dp110^{CAAX}$ alone or with $Toll^{10b}$. (C) Immunocytochemistry for Akt pS505 (green).

(D–G) r4-GAL4 was used to drive GFP or $Toll^{10b}$ in fat bodies of larvae heterozygous or hemizygous for $rictor^{\Delta 2}$. (D) Western blot analysis of Akt (pS505 and total) in whole-larval lysates, n = 2–4/gp. (E) Whole-animal triglycerides, n = 8/gp. *p = 0.0326 and **p = 0.0011 versus GFP. (F) Images of pupae. Scale bar, 2 mm. (G) Pupal body weights, n = 14–16/gp except $rictor^{\Delta 2}$/Y; r4-GAL4 > $Toll^{10b}$, n = 6. **p = 0.0020 and ****$p < 0.0001$ versus GFP. Data are presented as mean ± SD. See also Table S1.

co-expressing $Toll^{10b}$ and myrAkt had significantly larger nuclei than their WT neighbors (Figures 1I and 1J). Expression of myr-Akt also rescued triglyceride storage in larvae with active Toll signaling (Figure S2C). Together, these data show that Toll acts cell autonomously to block cell growth and triglyceride storage downstream of InR and upstream of Akt.

Toll Acts Independently of TORC2 to Block Insulin Signaling

Clonal expression of $Dp110^{CAAX}$, a constitutively active PI3K catalytic subunit, produced extremely large cells with massive nuclei. $Toll^{10b}$ co-expression blocked growth driven by $Dp110^{CAAX}$ (Figure 2A). We saw robust recruitment of the $PI(3,4,5)P_3$ reporter tGPH (Britton et al., 2002) to the plasma membrane of cells expressing $Dp110^{CAAX}$ alone or with $Toll^{10b}$, suggesting that the Toll pathway acts downstream of $PI(3,4,5)P_3$ to block insulin signaling (Figure 2B). Similarly, PI3K activation led to elevated Akt phospho-S505 signal in cells expressing $Dp110^{CAAX}$ alone or with $Toll^{10b}$ compared with surrounding WT cells (Figure 2C).

We formally tested whether mTORC2 mediates the ability of the Toll pathway to inhibit insulin signaling by asking whether $Toll^{10b}$ could reduce growth and nutrient storage in larvae lacking the essential mTORC2 component rictor. In *Drosophila*, null mutations in *rictor* abolish mTORC2 activity, block Akt S505 phosphorylation, and lead to a minor whole-animal growth defect (Hietakangas and Cohen, 2007; Lee and Chung, 2007). Akt S505 phosphorylation was undetectable in lysates of larvae hemizygous for the null allele $rictor^{\Delta 2}$ (Figure 2D). Nonetheless, fat body expression of $Toll^{10b}$ reduced triglyceride storage (Figure 2E) and whole-animal growth (Figures 2F and 2G) in $rictor^{\Delta 2}$ heterozygotes and hemizygotes.

Toll Signaling Acts at or Downstream of Pdk1 to Block Growth

Larvae homozygous for the strong hypomorphic $Pdk1^{\Delta 33}$ allele (Cheng et al., 2011) lack detectable phosphorylation of Akt T342 (Figure S1B) and weigh 60% less than heterozygotes. Expression of $Toll^{10b}$ in fat body reduced growth in $Pdk1^{\Delta 33}$ heterozygotes, but not homozygotes (Figures 3A and 3B). Fat bodies expressing $Toll^{10b}$ had elevated *Pdk1* mRNA levels compared with controls, a finding that was echoed for other insulin signaling intermediates (Figure S3). $Toll^{10b}$ expression had no effect on endogenous Pdk1 protein levels in fat body (Figure 3C), as measured using a *Pdk1* allele with a C-terminal myc tag, inserted using CRISPR/Cas9 (Figure S4).

The resistance of $Pdk1^{\Delta 33}$ homozygotes to the growth-reducing effects of fat body Toll signaling suggested that the Toll pathway targets Pdk1 to block insulin signaling. To test this hypothesis, we asked whether elevated Pdk1 expression could rescue $Toll^{10b}$-dependent phenotypes. GAL4-driven expression of Pdk1 in fat body clones led to increased cell and

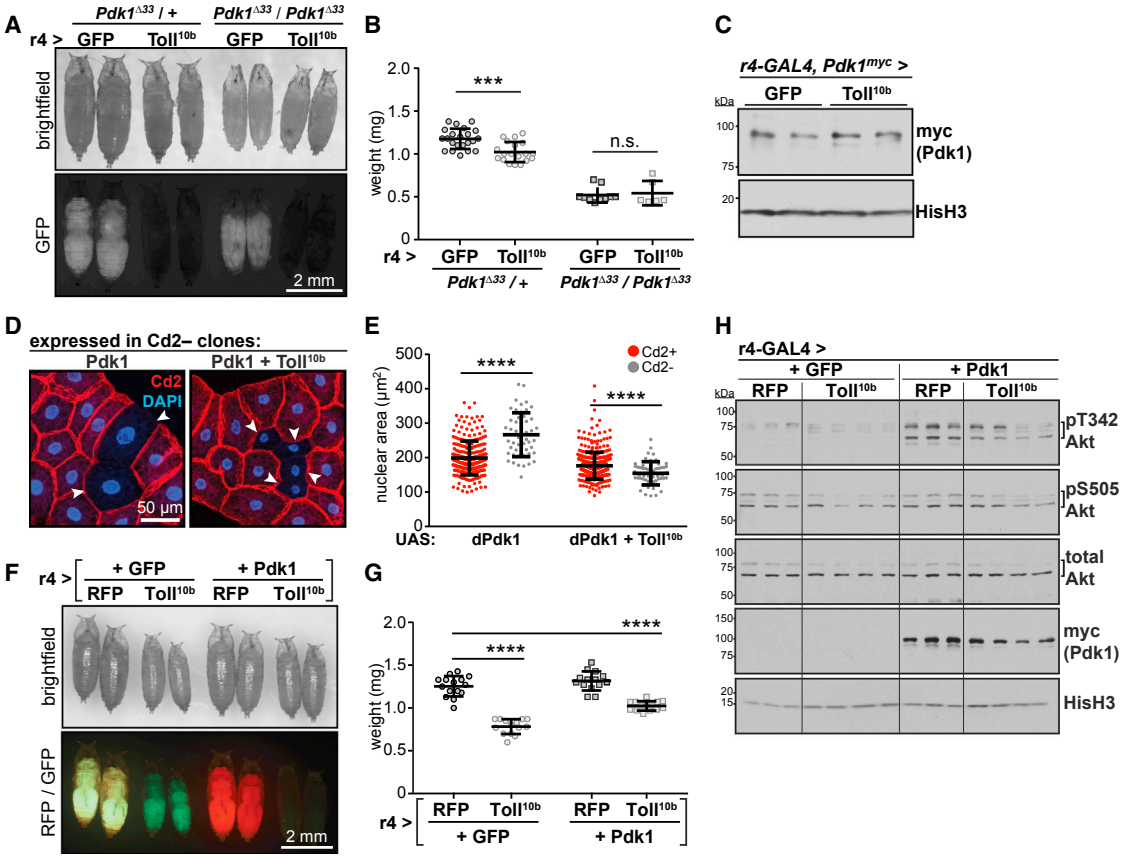

Figure 3. Toll Signaling Acts at or Downstream of Pdk1 to Block Growth

(A) Images of *Pdk1*$^{\Delta 33}$ mutant pupae expressing GFP or Toll^{10b} in fat body. Scale bar, 2 mm.

(B) Pupal body weights, n = 19–22/gp for *Pdk1*$^{\Delta 33}$/+, n = 6–10/gp for *Pdk1*$^{\Delta 33}$/*Pdk1*$^{\Delta 33}$. ***p = 0.0002 versus GFP.

(C) Western blot analysis of endogenous Pdk1 with a C-terminal myc tag (Pdk1^{myc}) in fat bodies expressing GFP or Toll^{10b}, n = 2/gp.

(D) Micrographs of fat bodies containing Cd2^{-}, GAL4^{+} cells (arrowheads) expressing Pdk1 (left) or Pdk1 + Toll^{10b} (right). WT cells are Cd2^{+} (red); nuclei are stained with DAPI (blue). Scale bar, 50 μm.

(E) Nuclear area in Cd2^{+}, GAL4^{-} cells (red, Pdk1, n = 262; Pdk1+Toll^{10b}, n = 379) and Cd2^{-}, GAL4^{+} cells (gray, Pdk1, n = 50; Pdk1+Toll^{10b}, n = 55). ****p < 0.0001 versus Cd2^{+}.

(F) Images of pupae. Scale bar, 2 mm.

(G) Pupal body weights, n = 14–15/gp. ****p = 0.0001 versus RFP + GFP.

(H) Western blot analysis of pT342, pS505, and total Akt, transgenically expressed Pdk1 (myc-tagged) and Histone H3 (HisH3) in fat bodies, n = 3–4/gp. Data are presented as mean ± SD. See also Table S1 and Figures S1, S3, and S4.

nuclear size. However, as with the InR^{A1325D} and Dp110^{CAAX} transgenes, this growth advantage was completely suppressed by co-expression of Toll^{10b} (Figures 3D and 3E). Animals expressing Toll^{10b} throughout the fat body, with or without Pdk1 co-expression, were smaller than controls (Figures 3F and 3G). Forced expression of Pdk1 drove Akt T342 phosphorylation relative to control fat bodies with no effect on phospho-S505 or total Akt levels. Toll signaling considerably reduced Pdk1-driven T342 phosphorylation without affecting Pdk1 transgene expression (Figure 3H).

Mimicking Akt Thr342 Phosphorylation Rescues Toll-Dependent Phenotypes

Toll signaling does not further reduce growth in *Pdk1* mutants, and yet elevated Pdk1 is insufficient to rescue growth in animals expressing Toll^{10b} in fat body. These results suggest that Toll signaling may inhibit Pdk1 activity or activate an Akt T342 phosphatase. Consequently, we asked whether expression of a phospho-mimicking T342D Akt mutant would rescue Toll^{10b}-dependent growth and nutrient storage phenotypes. Unlike InR^{A1325D}, Dp110^{CAAX}, Pdk1, and myrAkt, Akt^{T342D} did not increase nuclear area when expressed in fat body cells. However, Akt^{T342D} expression substantially rescued growth in fat body cells co-expressing Toll^{10b} (Figures 4A and 4B). Co-expression of Toll^{10b} with Akt^{T342D}, but not with WT Akt, rescued impaired triglyceride storage caused by innate immune signaling (Figures 4C and 4D). Expression of the Akt^{T342D} transgene completely rescued the whole-animal growth defect caused by fat body Toll signaling (Figures 4E and 4F). The majority of flies that express Toll^{10b} in fat body die just before eclosion. This reduced viability can be rescued by loss of the Toll pathway transcription factor Dif or by expression of Akt^{T342D}, but not by

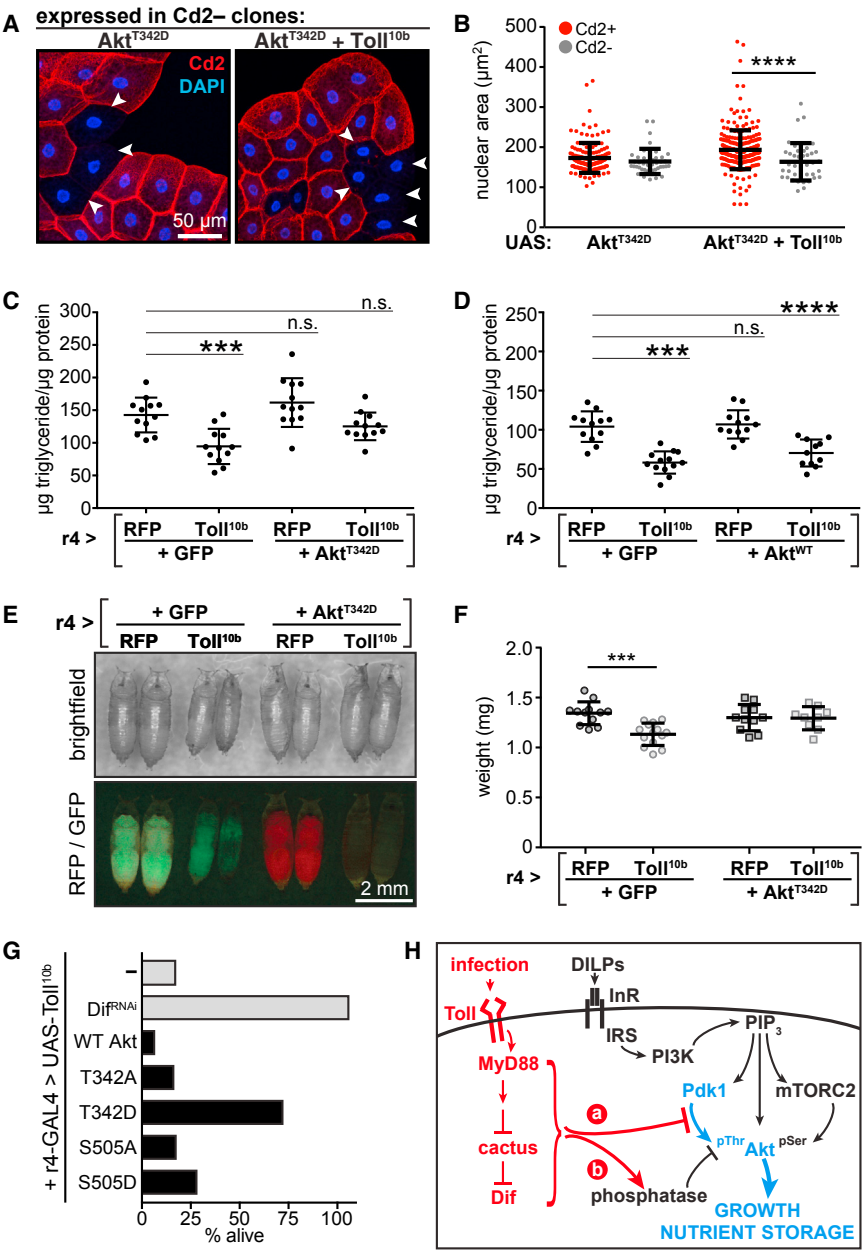

Figure 4. Mimicking Akt Thr342 Phosphorylation Rescues Toll-Dependent Phenotypes

(A) Micrographs of fat bodies containing Cd2$^-$, GAL4$^+$ cells (arrowheads) expressing Akt^{T342D} (left) or Akt^{T342D} + Toll^{10b} (right). WT cells are Cd2$^+$ (red); nuclei are stained with DAPI (blue). Scale bar, 50 μm.

(B) Nuclear area in Cd2$^+$, GAL4$^-$ cells (red, Akt^{T342D}, n = 138; Akt^{T342D}+Toll^{10b}, n = 260), and Cd2$^-$, GAL4$^+$ cells (gray, Akt^{T342D}, n = 42; Akt^{T342D}+Toll^{10b}, n = 40). ****p < 0.0001 versus Cd2$^+$.

(C and D) Whole-animal triglycerides in animals expressing Toll^{10b} in fat body with Akt^{T342D} (C) or WT Akt (D), n = 11–13/gp. ***p = 0.0005 and ****p < 0.0001 versus RFP + GFP.

(E) Images of pupae. Scale bar, 2 mm.

(F) Pupal body weights, n = 9–14/gp. ***p = 0.0001 versus RFP + GFP.

(G) Percent recovery of viable adult r4-GAL4, UAS-Toll^{10b} flies co-expressing indicated transgenes in fat body, n = 78–146 adults/cross. Data in (B), (C), (D), and (F) are presented as mean ± SD. See also Table S1.

(H) Model for inhibition of T342 phosphorylation by Toll signaling.

transgenes encoding WT, S505D, T342A, or S505A Akt (Figure 4G). Together, these data suggest that the reduction in insulin signaling, growth, and nutrient storage in cells with active Toll signaling is due to inhibition of Akt T342 phosphorylation.

DISCUSSION

Using a genetic approach, we show that Toll signaling acts in a cell-autonomous manner to inhibit insulin signaling downstream of IRS/chico and PI3K. Constitutive PI3K activity drives PI(3,4,5)P_3 accumulation and mTORC2 activity in cells expressing Toll^{10b}, but these two signaling events are uncoupled from cell growth when the Toll pathway is active. Our data indicate that Akt phosphorylation on the Pdk1 site, T342, is the critical step regulated by Toll signaling. Our data fit the consensus in the literature that phosphorylation on the activation loop (T342) rather than on the hydrophobic motif (S505) is the more critical step for insulin signaling. First, we find that elevated Pdk1 expression robustly drives cell growth and T342 phosphorylation without affecting S505 phosphorylation or total Akt levels. Second, loss of *rictor* leads to minor growth defects compared with loss of *Pdk1* (this study; Cheng et al., 2011; Hietakangas and Cohen, 2007; Lee and Chung, 2007). Third, loss of mTORC2 components in mice blocks mAkt S473 phosphorylation, but this affects only a subset of Akt targets (Guertin et al., 2006; Jacinto et al., 2006; Kumar et al., 2010). Finally, mAkt T308 phosphorylation promotes full Akt activity via activation of mTORC2 and subsequent S473 phosphorylation (Yang et al., 2015).

Toll signaling does not reduce Pdk1 or Akt levels, and future work will be required to determine whether regulation of T342 phosphorylation occurs through impaired interaction between Pdk1 and Akt, reduced Pdk1 activity, or increased phosphatase activity toward T342 (Figure 4H). Mammalian Akt is subject to post-translational modifications that regulate translocation to the plasma membrane and, consequently, interaction with Pdk1 (Risso et al., 2015). Pdk1 activity is regulated by subcellular localization, activating tyrosine phosphorylation, and autophosphorylation that reduces homodimerization and increases

activity toward Akt (Calleja et al., 2014). The phosphatases PP2A and Phlpp dephosphorylate mAkt1 (Gao et al., 2005; Kuo et al., 2008), but knockdown of *Phlpp* fails to rescue growth in fat body cells expressing Toll^{10b} (data not shown).

Elevated Pdk1 expression drives Akt T342 phosphorylation, and Toll signaling impairs this, albeit incompletely. Nonetheless, fat body Toll signaling blocks growth in animals co-expressing the Pdk1 transgene, but not in those co-expressing Akt^{T342D}. Several possibilities could account for these results. First, there may be discordance between experimentally observable Akt phosphorylation and the activity of its growth-promoting substrates such that maximal Akt activity, achieved in the absence of Toll signaling, is needed for InR^{A1325D}, Dp110^{CAAX}, and Pdk1 transgenes to drive growth. Indeed, our results with these transgenes indicate a considerable reserve capacity for Akt activity and cell growth *in vivo*. Second, the Toll and insulin signaling pathways may operate in parallel to regulate a downstream target critical for growth, and the Akt^{T342D} transgene may more efficiently correct downstream signaling compared with the Pdk1 transgene. Third, fat bodies that co-express Pdk1 and Toll^{10b} might maintain relatively elevated Akt T342 phosphorylation because of the kinetics of induction of negative regulators of Pdk1 and/or T342 phosphorylation. Future work will be required to distinguish among these possibilities.

Toll signaling in the fat body acts not only cell autonomously to disrupt insulin signaling, but also cell nonautonomously to reduce whole-animal growth. Hemolymph Dilp2 levels are not changed by Toll signaling, suggesting that reduced whole-animal growth caused by fat body Toll signaling may be due to peripheral insulin resistance and not impaired Dilp secretion from insulin-producing cells. Similarly, in mice, loss of insulin signaling in adipose tissue leads to insulin resistance in liver and muscle (Abel et al., 2001; Kumar et al., 2010; Shearin et al., 2016; Softic et al., 2016). A major question arising from these studies and ours is the following: what mechanisms communicate a reduction in insulin signaling in one organ to the rest of the animal? Genetic screens in model organisms such as *Drosophila* may pave the way for addressing this outstanding matter.

In conclusion, our findings demonstrate that Toll signaling disrupts insulin signaling downstream of IRS, PI3K, and Pdk1 by interfering with Akt phosphorylation on its activation loop site. Our results echo findings in mammalian cells that many treatments that provoke insulin resistance do so independently of IRS and through a variety of mechanisms (Hoehn et al., 2008). Furthermore, our results define the point in the insulin signaling pathway that is blocked by Toll signaling and provide a genetic model with robust phenotypes that can be used to identify the cell-autonomous and cell-nonautonomous mechanisms employed by the Toll pathway to disrupt insulin signaling.

EXPERIMENTAL PROCEDURES

Drosophila Stocks and Husbandry

Flies were raised on standard food at 25°C, and 6- to 8-hr egg lays were conducted to prevent overcrowding. Experiments were performed using mid-third-instar larvae (96–108 hr after egg lay) or white prepupae (0–5 hr after puparium formation). Stocks used in this study, the UAS-Akt^{T342D} and UAS-Pdk1 transgenes, and the CRISPR/Cas9 strategy used to generate a myc-tagged *Pdk1* allele are described in Supplemental Experimental Procedures. Full genotypes are listed in Table S1.

Antibodies and Western Blotting

Sources and dilutions of primary and secondary antibodies used in this study are listed in Supplemental Experimental Procedures. The rabbit anti-phosphoThr342-Akt antibody was generated against the phosphopeptide YGRTTK(Tp)FCGTPE. Peptide synthesis, immunization, and antibody purification were performed at Alpha Diagnostics International (San Antonio, TX). Western blotting was performed using larval or fat body lysates as described in Supplemental Experimental Procedures.

Mosaic Analysis of Cell Size

Act5c > *Cd2* > *GAL4* flies were crossed to *hsFLP* flies carrying UAS transgenes. After overnight egg lays, embryos were heat shocked (37°C, 45 min) to induce FLP recombinase. Larval fat bodies were subjected to immunostaining for Cd2 as described in Supplemental Experimental Procedures. *Z*-stack images (2 μm interval) were collected on a Perkin Elmer UltraVIEW High Speed Confocal Imaging microscope with Volocity software or a Zeiss LSM 700 confocal microscope with ZEN imaging software. Maximum intensity projection images were colorized in Adobe Photoshop. For analysis of nuclear area, images of DAPI-stained nuclei were imported into ImageJ and subjected to thresholding, and nuclear area was calculated in Cd2$^+$ and Cd2$^-$ cells.

Dilp2, Triglyceride, and Animal Weight Measurements

Hemolymph was collected on ice from 10 to 12 larvae, and 1 μL of pooled hemolymph was used for Dilp2 measurement by ELISA (Park et al., 2014). Triglycerides were measured as described (Bland et al., 2010). Pupae were weighed in groups of 4–6 following removal of food from the cuticle.

Statistics

Statistical analyses were performed using GraphPad Prism 7. Sample sizes (referring to biological replicates of cells or animals) are listed in the figure legends. Unpaired two-tailed t tests were used to assess differences in nuclear area between Cd2$^+$, GAL4$^-$, and Cd2$^-$, GAL4$^+$ cells and between *rictor*$^{\Delta 2}$ and *Pdk1*$^{\Delta 33}$ heterozygotes or homo/hemizygotes expressing GFP or Toll^{10b} in fat body. For other triglyceride and body weight experiments, one-way ANOVA was used to determine differences between groups.

SUPPLEMENTAL INFORMATION

Supplemental Information includes Supplemental Experimental Procedures, four figures, and one table and can be found with this article online at https://doi.org/10.1016/j.celrep.2018.02.033.

ACKNOWLEDGMENTS

We thank Tony Ip (University of Massachusetts, Worcester) and Graeme Davis (UCSF) for fly stocks, Mazhar Adli (University of Virginia) for advice on the CRISPR/Cas9 strategy, Young Jun Lee and Miyuki Suzawa for technical assistance, members of the Bland lab for discussions, and the Bloomington *Drosophila* Stock Center and the *Drosophila* Genomics Research Center for reagents. This work was supported by NIH Grants R21DK089391 to M.J.B. and R01DK099601 to M.L.B.

AUTHOR CONTRIBUTIONS

Conceptualization, M.J.B. and M.L.B.; Methodology, M.L.B.; Investigation, S.W.R., M.D.B., and M.L.B.; Writing, M.L.B.; Funding Acquisition, M.J.B. and M.L.B.

DECLARATION OF INTERESTS

M.J.B. is a full-time employee of Pfizer, Inc.

Received: December 20, 2017
Revised: February 6, 2018
Accepted: February 8, 2018
Published: March 6, 2018

REFERENCES

Abel, E.D., Peroni, O., Kim, J.K., Kim, Y.B., Boss, O., Hadro, E., Minnemann, T., Shulman, G.I., and Kahn, B.B. (2001). Adipose-selective targeting of the GLUT4 gene impairs insulin action in muscle and liver. Nature *409*, 729–733.

Arrese, E.L., and Soulages, J.L. (2010). Insect fat body: energy, metabolism, and regulation. Annu. Rev. Entomol. *55*, 207–225.

Bland, M.L., Lee, R.J., Magallanes, J.M., Foskett, J.K., and Birnbaum, M.J. (2010). AMPK supports growth in *Drosophila* by regulating muscle activity and nutrient uptake in the gut. Dev. Biol. *344*, 293–303.

Boura-Halfon, S., and Zick, Y. (2009). Phosphorylation of IRS proteins, insulin action, and insulin resistance. Am. J. Physiol. Endocrinol. Metab. *296*, E581–E591.

Britton, J.S., Lockwood, W.K., Li, L., Cohen, S.M., and Edgar, B.A. (2002). *Drosophila*'s insulin/PI3-kinase pathway coordinates cellular metabolism with nutritional conditions. Dev. Cell *2*, 239–249.

Brogiolo, W., Stocker, H., Ikeya, T., Rintelen, F., Fernandez, R., and Hafen, E. (2001). An evolutionarily conserved function of the *Drosophila* insulin receptor and insulin-like peptides in growth control. Curr. Biol. *11*, 213–221.

Buchon, N., Silverman, N., and Cherry, S. (2014). Immunity in *Drosophila melanogaster*—from microbial recognition to whole-organism physiology. Nat. Rev. Immunol. *14*, 796–810.

Calleja, V., Laguerre, M., de Las Heras-Martinez, G., Parker, P.J., Requejo-Isidro, J., and Larijani, B. (2014). Acute regulation of PDK1 by a complex interplay of molecular switches. Biochem. Soc. Trans. *42*, 1435–1440.

Cheng, L., Locke, C., and Davis, G.W. (2011). S6 kinase localizes to the presynaptic active zone and functions with PDK1 to control synapse development. J. Cell Biol. *194*, 921–935.

Copps, K.D., Hançer, N.J., Opare-Ado, L., Qiu, W., Walsh, C., and White, M.F. (2010). Irs1 serine 307 promotes insulin sensitivity in mice. Cell Metab. *11*, 84–92.

Copps, K.D., Hançer, N.J., Qiu, W., and White, M.F. (2016). Serine 302 phosphorylation of mouse insulin receptor substrate 1 (IRS1) is dispensable for normal insulin signaling and feedback regulation by hepatic S6 kinase. J. Biol. Chem. *291*, 8602–8617.

DiAngelo, J.R., Bland, M.L., Bambina, S., Cherry, S., and Birnbaum, M.J. (2009). The immune response attenuates growth and nutrient storage in *Drosophila* by reducing insulin signaling. Proc. Natl. Acad. Sci. USA *106*, 20853–20858.

Dionne, M.S., Pham, L.N., Shirasu-Hiza, M., and Schneider, D.S. (2006). Akt and FOXO dysregulation contribute to infection-induced wasting in *Drosophila*. Curr. Biol. *16*, 1977–1985.

Gao, T., Furnari, F., and Newton, A.C. (2005). PHLPP: a phosphatase that directly dephosphorylates Akt, promotes apoptosis, and suppresses tumor growth. Mol. Cell *18*, 13–24.

Géminard, C., Rulifson, E.J., and Léopold, P. (2009). Remote control of insulin secretion by fat cells in *Drosophila*. Cell Metab. *10*, 199–207.

Guertin, D.A., Stevens, D.M., Thoreen, C.C., Burds, A.A., Kalaany, N.Y., Moffat, J., Brown, M., Fitzgerald, K.J., and Sabatini, D.M. (2006). Ablation in mice of the mTORC components raptor, rictor, or mLST8 reveals that mTORC2 is required for signaling to Akt-FOXO and PKCalpha, but not S6K1. Dev. Cell *11*, 859–871.

Hietakangas, V., and Cohen, S.M. (2007). Re-evaluating AKT regulation: role of TOR complex 2 in tissue growth. Genes Dev. *21*, 632–637.

Hoehn, K.L., Hohnen-Behrens, C., Cederberg, A., Wu, L.E., Turner, N., Yuasa, T., Ebina, Y., and James, D.E. (2008). IRS1-independent defects define major nodes of insulin resistance. Cell Metab. *7*, 421–433.

Jacinto, E., Facchinetti, V., Liu, D., Soto, N., Wei, S., Jung, S.Y., Huang, Q., Qin, J., and Su, B. (2006). SIN1/MIP1 maintains rictor-mTOR complex integrity and regulates Akt phosphorylation and substrate specificity. Cell *127*, 125–137.

Jia, L., Vianna, C.R., Fukuda, M., Berglund, E.D., Liu, C., Tao, C., Sun, K., Liu, T., Harper, M.J., Lee, C.E., et al. (2014). Hepatocyte Toll-like receptor 4 regulates obesity-induced inflammation and insulin resistance. Nat. Commun. *5*, 3878.

Kumar, A., Lawrence, J.C., Jr., Jung, D.Y., Ko, H.J., Keller, S.R., Kim, J.K., Magnuson, M.A., and Harris, T.E. (2010). Fat cell-specific ablation of rictor in mice impairs insulin-regulated fat cell and whole-body glucose and lipid metabolism. Diabetes *59*, 1397–1406.

Kuo, Y.-C., Huang, K.-Y., Yang, C.-H., Yang, Y.-S., Lee, W.-Y., and Chiang, C.-W. (2008). Regulation of phosphorylation of Thr-308 of Akt, cell proliferation, and survival by the B55alpha regulatory subunit targeting of the protein phosphatase 2A holoenzyme to Akt. J. Biol. Chem. *283*, 1882–1892.

Lackey, D.E., and Olefsky, J.M. (2016). Regulation of metabolism by the innate immune system. Nat. Rev. Endocrinol. *12*, 15–28.

Lee, G., and Chung, J. (2007). Discrete functions of rictor and raptor in cell growth regulation in *Drosophila*. Biochem. Biophys. Res. Commun. *357*, 1154–1159.

Libert, S., Chao, Y., Zwiener, J., and Pletcher, S.D. (2008). Realized immune response is enhanced in long-lived puc and chico mutants but is unaffected by dietary restriction. Mol. Immunol. *45*, 810–817.

Park, S., Alfa, R.W., Topper, S.M., Kim, G.E.S., Kockel, L., and Kim, S.K. (2014). A genetic strategy to measure circulating *Drosophila* insulin reveals genes regulating insulin production and secretion. PLoS Genet. *10*, e1004555.

Risso, G., Blaustein, M., Pozzi, B., Mammi, P., and Srebrow, A. (2015). Akt/PKB: one kinase, many modifications. Biochem. J. *468*, 203–214.

Saberi, M., Woods, N.-B., de Luca, C., Schenk, S., Lu, J.C., Bandyopadhyay, G., Verma, I.M., and Olefsky, J.M. (2009). Hematopoietic cell-specific deletion of Toll-like receptor 4 ameliorates hepatic and adipose tissue insulin resistance in high-fat-fed mice. Cell Metab. *10*, 419–429.

Shearin, A.L., Monks, B.R., Seale, P., and Birnbaum, M.J. (2016). Lack of AKT in adipocytes causes severe lipodystrophy. Mol. Metab. *5*, 472–479.

Softic, S., Boucher, J., Solheim, M.H., Fujisaka, S., Haering, M.-F., Homan, E.P., Winnay, J., Perez-Atayde, A.R., and Kahn, C.R. (2016). Lipodystrophy due to adipose tissue-specific insulin receptor knockout results in progressive NAFLD. Diabetes *65*, 2187–2200.

Tao, C., Holland, W.L., Wang, Q.A., Shao, M., Jia, L., Sun, K., Lin, X., Kuo, Y.-C., Johnson, J.A., Gordillo, R., et al. (2017). Short-term versus long-term effects of adipocyte Toll-like receptor 4 activation on insulin resistance in male mice. Endocrinology *158*, 1260–1270.

Weisberg, S.P., McCann, D., Desai, M., Rosenbaum, M., Leibel, R.L., and Ferrante, A.W., Jr. (2003). Obesity is associated with macrophage accumulation in adipose tissue. J. Clin. Invest. *112*, 1796–1808.

Xu, H., Barnes, G.T., Yang, Q., Tan, G., Yang, D., Chou, C.J., Sole, J., Nichols, A., Ross, J.S., Tartaglia, L.A., and Chen, H. (2003). Chronic inflammation in fat plays a crucial role in the development of obesity-related insulin resistance. J. Clin. Invest. *112*, 1821–1830.

Yang, G., Murashige, D.S., Humphrey, S.J., and James, D.E. (2015). A positive feedback loop between Akt and mTORC2 via SIN1 phosphorylation. Cell Rep. *12*, 937–943.

Cell Reports, Volume *22*

Supplemental Information

Innate Immune Signaling in *Drosophila* Blocks Insulin Signaling by Uncoupling $PI(3,4,5)P_3$ Production and Akt Activation

Stephen W. Roth, Moshe D. Bitterman, Morris J. Birnbaum, and Michelle L. Bland

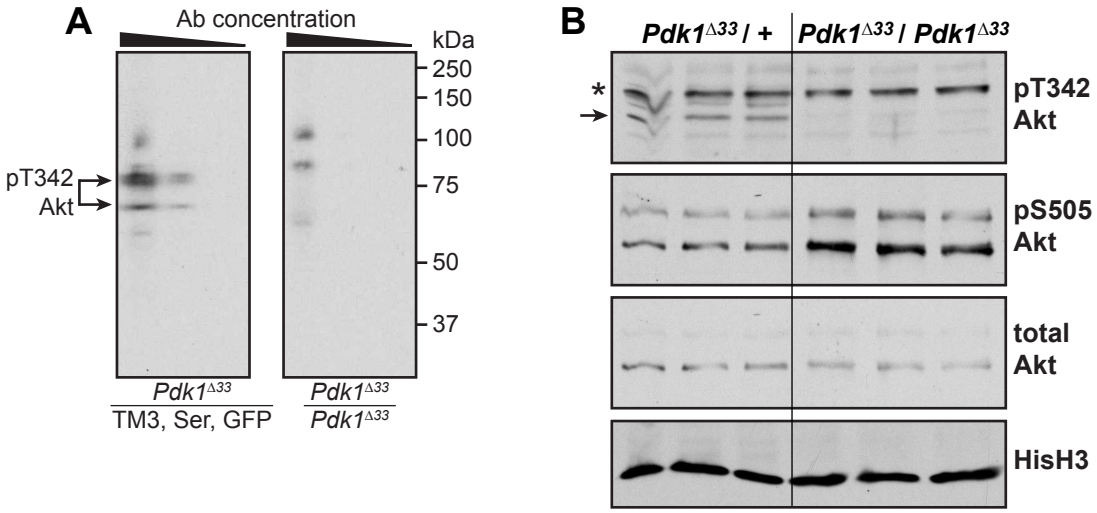

Figure S1. Validation of a novel rabbit anti-phosphoThr342-Akt antibody, Related to Figures 1 and 3. **A)** A rabbit anti-phosphoThr342-Akt antibody was raised against a phosphorylated peptide and affinity purified. Serial dilutions of anti-sera were tested against lysates from larvae heterozygous (left) or homoozygous (right) for the strong, hypomorphic *Pdk1*$^{\Delta 33}$ mutation. The antibody detects signal in *Pdk1*$^{\Delta 33}$ heterozygotes but not homozygotes at ~66 and 85 kDa (arrows), consistent with the reported molecular weights of Akt splice variants (Andjelkovic et al., 1995). **B)** Western blot analysis of phosphorylated (pT342 and pS505) and total Akt and Histone H3 (HisH3) in larvae heterozygous (left, n = 2 animals/lane) or homozygous (right, n = 10 animals/lane) for *Pdk1*$^{\Delta 33}$. The arrow points to phospho-T342 Akt, the higher molecular weight band (*) is non-specific.

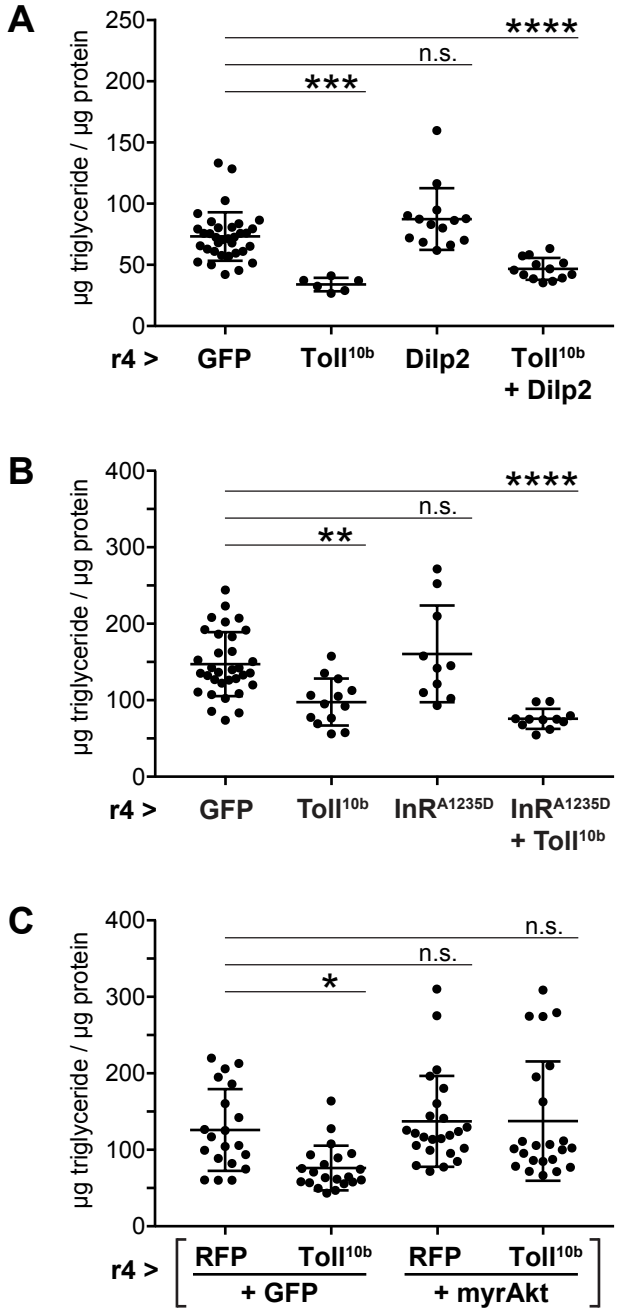

Figure S2. Toll signaling acts downstream of the insulin receptor and upstream of Akt to suppress triglyceride storage, Related to Figure 1.

Triglyceride levels were measured and normalized to protein in whole animal lysates of mid-third instar larvae expressing the following transgenes in fat body under control of r4-GAL4: **A)** GFP, Toll^{10b}, Dilp2, or Toll^{10b} + Dilp2, n = 6-14/gp, except GFP, n = 34, ****p < 0.0001 and ***p = 0.0002 versus GFP; **B)** GFP, Toll^{10b}, InR^{A1325}, or InR^{A1325} + Toll^{10b}, n = 10-13/gp, except GFP, n = 33, **p = 0.0013 and ****p < 0.0001 versus GFP; **C)** RFP + GFP, Toll^{10b} + GFP, RFP + myrAkt, or Toll^{10b} + myrAkt, n = 20-23/gp, *p = 0.0207 versus RFP+GFP. Data are presented as mean ± S.D.

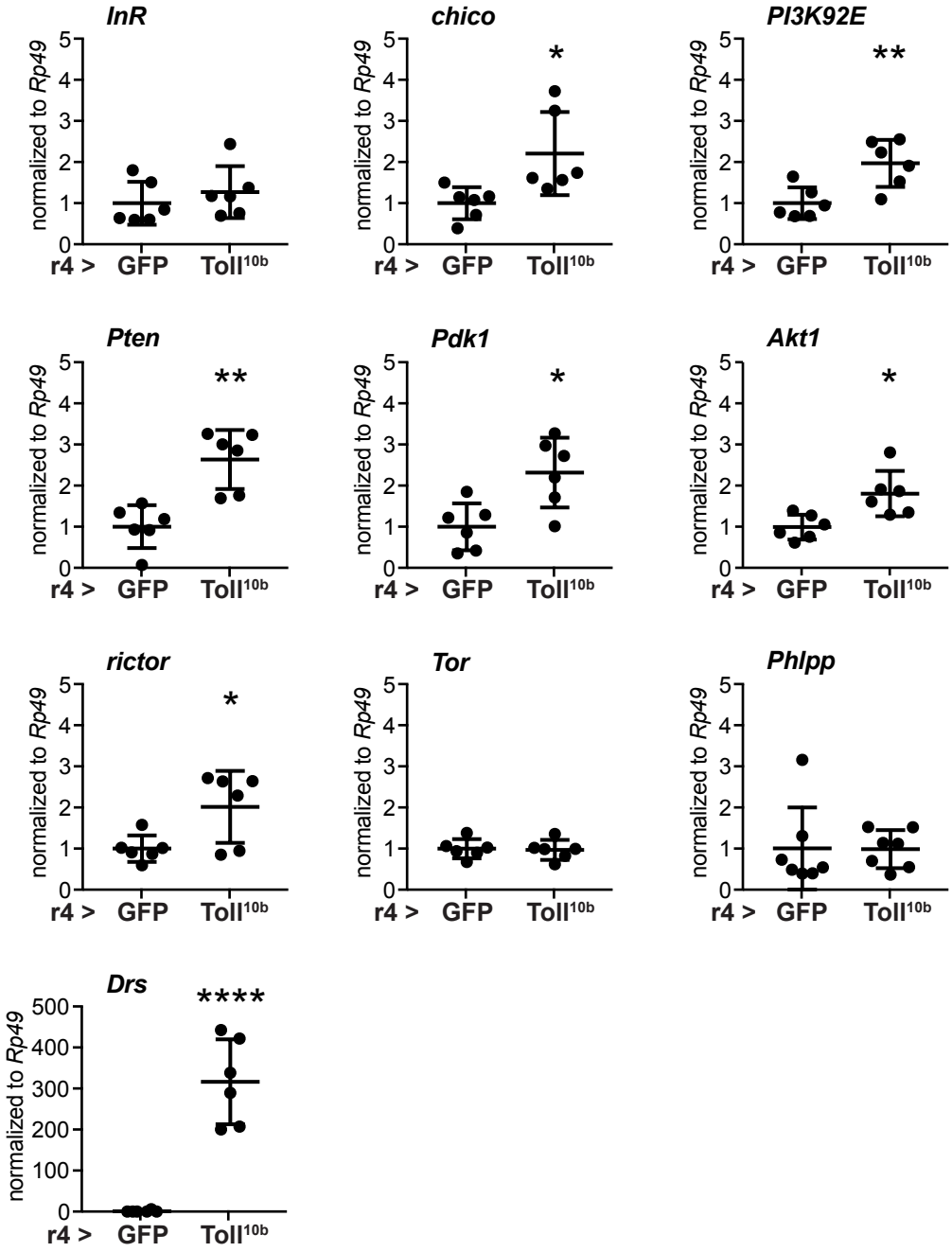

Figure S3. Insulin signaling pathway gene expression in fat bodies with active Toll signaling, Related to Figure 3.

RNA was isolated from mid-third instar larval fat bodies expressing GFP or Toll^{10b} under control of r4-GAL4. Transcript levels of *InR*, *chico*, *PI3K92E* (encodes Dp110), *Pten*, *Pdk1*, *Akt1*, *rictor*, *Tor*, *Phlpp* and *Drs* were measured in equal amounts of cDNA by Q-PCR. All transcripts are normalized to *Rp49* levels, which did not differ between genotypes. *Drs* encodes Drosomycin, a canonical antimicrobial peptide target gene of the Toll signaling pathway. *$p < 0.05$, **$p < 0.01$ and ****$p < 0.0001$ versus GFP, n = 6-7 samples/genotype. Data are presented as mean ± S.D.

A ***Pdk1*, 3' exons**

B **Wild type allele**

GCTATGCTATCCACTGGTCGGAAGCTATTGAGAACATGCGCAAGTTGGCCTACGGAGATCCCTCCTCCACATCTGCAGT
GTCCTGCTCCAGCGGCAGCAGTAATAGCCTGGCTGTCATCTCAAATTCATCCGCCGCCTCCTCAAGCAATTCGCCCACG
GTGAAACGCAGTTCCCCCGTAAACGCTCCTCAAGCTTCGACGGCGTCTGACAACCGGACATTGGGTAGCACCAGAACGG
G**GACGTCACCTAGCAAGAAGACGG**CGTCTAAG**TAA**ACGTAGTCCTATTTATAGCAATGTGAAATTAATTTAGTTGAAAT
TTAGTGCAAACGAAGCGATGGCGTAGAAGAGGGCGGGAATAGAAGTAAGCTTAGAAGTAGAAGTAAGTGATGAAGGGGA
AATAATGATCGTGTCTCTAGTGCTAATTAGAACCAAATTTCTGTTTTCCGATTTGTATTGTGCTTAGGGCG

ssDNA template for homology-directed repair

AGCTTCGACGGCGTCTGACAACCGGACATTGGGTAGCACCAGAACGGG**GACGTCACCTAGCAAGAAGAC*AA***CGTCTAAG
ATGGAGCAGAAGCTGATCTCCGAGGAGGATCTGTAAATAACGTAGTCCTATTTATAGCAATGTGAAATTAATTTAGTTG
AAATTTAGTGCAAACGAAGCGATGGCGTAGAAGAGGGCGGGA

Modified allele

GCTATGCTATCCACTGGTCGGAAGCTATTGAGAACATGCGCAAGTTGGCCTACGGAGATCCCTCCTCCACATCTGCAGT F1
GTCCTGCTCCAGCGGCAGCAGTAATAGCCTGGCTGTCATCTCAAATTCATCCGCCGCCTCCTCAAGCAATTCGCCCACG
GTGAAACGCAGTTCCCCCGTAAACGCTCCTCAAGCTTCGACGGCGTCTGACAACCGGACATTGGGTAGCACCAGAACGG
G**GACGTCACCTAGCAAGAAGAC*AA***CGTCTAAG**ATGGAGC**AGAAGCTGATCTCCGAGGAG**GATCTG**TAA**ATAACG**TAG**TC R2
CTATTTATAGCAATGTGAAATTAATTTAGTTGAAATTTAGTGCAAACGAAGCGATGGCGTAGAAGAGGGCGGGAATAGA
AGTAAGCTTAGAAGTAGAAGTAAGTGATGAAGGGGAAATAATGATCGTGTCTCTAGTGCTAATTAGAACCAAATTTCTG
TTTTCCGATTTGTATTGTGCTTAGGGCG R1

C

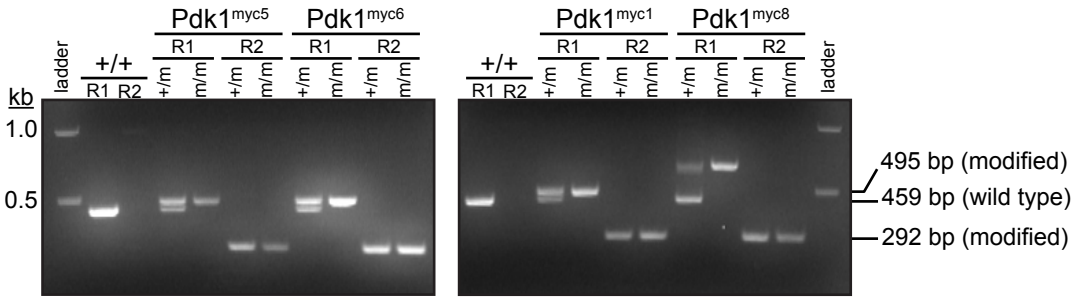

D

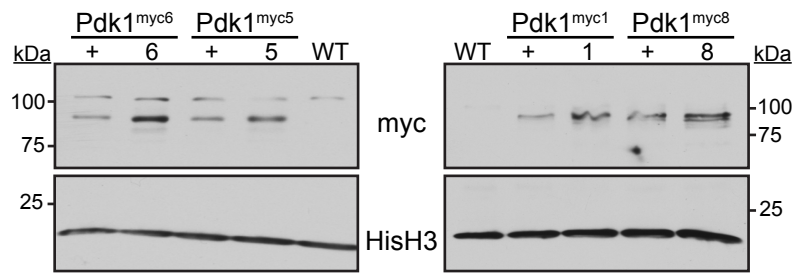

E

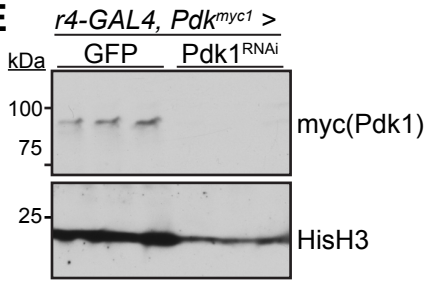

Figure S4. Design and validation of a CRISPR/Cas9 strategy to insert a myc tag at the 3' end of the *Pdk1* coding region, Related to Figure 3.

A) The final coding exons (black) and 3'UTR (gray) of *Pdk1* are depicted. The region underlined in blue corresponds to the DNA sequence in part B and is common to all *Pdk1* splice variants. Numbering above exons refers to coordinates in FlyBase release 6.10. **B)** Top: the final 272 nt encoding the carboxy-terminus of wild type *Pdk1* and the first 194 nt of the 3'UTR. Middle: the sequence of the ssDNA template for homology-directed repair following DNA cleavage by Cas9. The gRNA sequence is in bold text and underlined. Stop codons are in red, and the sequence encoding the myc tag is in blue. The 79 bp (left) and 81 bp (right) homology arms of the ssDNA oligo are highlighted in gray. Bottom: the expected DNA sequence of the targeted *Pdk1* allele. Note the mutated PAM site (italicized) present in both the ssDNA oligo and the targeted allele. Primer sequences (F1, R1, and R2) used in part C are boxed. **C)** PCR genotyping of wild type (+/+), $Pdk1^{myc}$/+, and $Pdk1^{myc}$/$Pdk1^{myc}$ flies is shown for four independent insertions: lines 5, 6, 1, and 8. Line 8 contains multiple copies of the myc insertion. **D, E)** Western blot analysis of myc (Pdk1) and HisH3 levels in **D)** adult flies that are wild type (WT), heterozygous, or homozygous for $Pdk1^{myc6}$, $Pdk1^{myc5}$, $Pdk1^{myc1}$, or $Pdk1^{myc8}$ (n = 2 flies/lane) and **E)** larval fat bodies heterozygous for $Pdk1^{myc1}$ and expressing GFP or a $Pdk1^{RNAi}$ transgene under control of the fat body driver r4-GAL4 (n = 3/gp, 10 fat bodies pooled/lane).

Figure	Genotype
1A	*w; UAS-GFP / +; r4-GAL4 / +* and *w; UAS-Toll^{10b} / +; r4-GAL4 / +*
1B	*w;* [*UAS-GFP* or *UAS-Toll^{10b}*] */ +; r4-GAL4, dilp2^{1}, gd2HF / dilp2^{1}, gd2HF*
1C	*w; UAS-GFP/+; r4-GAL4 / +* and *w; +/+; r4-GAL4/UAS-Dilp2* and *w; UAS-Toll^{10b}/+; r4-GAL4/UAS-Dilp2*
1E, left	*y, w, hsFLP / w; +/+; Act5c>Cd2>GAL4 / +*
1E, right	*y, w, hsFLP / w; +/+; Act5c>Cd2>GAL4 / UAS-Toll^{10b}*
1G, left	*y, w, hsFLP / w; UAS-InR^{A1325D} / +; Act5c>Cd2>GAL4 / +*
1G, right	*y, w, hsFLP / w; UAS-InR^{A1325D}, UAS-Toll^{10b} / +; Act5c>Cd2>GAL4 / +*
1I, left	*y, w, hsFLP / w; +/+; Act5c>Cd2>GAL4 / UAS-myrAkt*
1I, right	*y, w, hsFLP / w; UAS-Toll^{10b} / +; Act5c>Cd2>GAL4 / UAS-myrAkt*
2A-C, left	*y, w, hsFLP, UAS-Dp110^{CAAX} / w; + / +; Act5c>Cd2>GAL4 / +*
2A-C, right	*y, w, hsFLP, UAS-Dp110^{CAAX} / w; + / +; Act5c>Cd2>GAL4 / UAS-Toll^{10b}*
2D-G,	*rictor$^{\Delta 2}$ / +; +/+; r4-GAL4 / UAS-GFP*
left to right	*rictor$^{\Delta 2}$ / +; +/+; r4-GAL4 / UAS-Toll^{10b}*
	rictor$^{\Delta 2}$ / Y; +/+; r4-GAL4 / UAS-GFP
	rictor$^{\Delta 2}$ / Y; +/+; r4-GAL4 / UAS-Toll^{10b}
3A and B,	*w; UAS-GFP / +; r4-GAL4, Pdk1$^{\Delta 33}$/ TM3, Ser, GFP*
left to right	*w; UAS-Toll^{10b} / +; r4-GAL4, Pdk1$^{\Delta 33}$/ TM3, Ser, GFP*
	w; UAS-GFP / +; r4-GAL4, Pdk1$^{\Delta 33}$/ Pdk1$^{\Delta 33}$
	w; UAS-Toll^{10b} / +; r4-GAL4, Pdk1$^{\Delta 33}$/ Pdk1$^{\Delta 33}$
3C, left	*w; UAS-GFP / +; r4-GAL4 / Pdk1^{myc}*
3C, right	*w; UAS-Toll^{10b} / +; r4-GAL4 / Pdk1^{myc}*
3D, left	*y, w, hsFLP / w; + / +; Act5c>Cd2>GAL4 / UAS-Pdk1*
3D, right	*y, w, hsFLP / w; UAS- Toll^{10b} / +; Act5c>Cd2>GAL4 / UAS-Pdk1*
3F-H,	*w; UAS-RFP / +; r4-GAL4 / UAS-GFP*
left to right	*w; UAS-Toll^{10b} / +; r4-GAL4 / UAS-GFP*
	w; UAS-RFP / +; r4-GAL4 / UAS-Pdk1
	w; UAS-Toll^{10b} / +; r4-GAL4 / UAS-Pdk1
4A, left	*y, w, hsFLP / w; +/+; Act5c>Cd2>GAL4 / UAS-Akt^{T342D}*
4A, right	*y, w, hsFLP / w; UAS-Toll^{10b} / +; Act5c>Cd2>GAL4 / UAS-Akt^{T342D}*
4C & E, F	*w; UAS-RFP / +; r4-GAL4 / UAS-GFP*
left to right	*w; UAS-Toll^{10b} / +; r4-GAL4 / UAS-GFP*
	w; UAS-RFP / +; r4-GAL4 / UAS-Akt^{T342D}
	w; UAS-Toll^{10b} / +; r4-GAL4 / UAS-Akt^{T342D}
4D	*w; UAS-RFP / +; r4-GAL4 / UAS-GFP*
left to right	*w; UAS-Toll^{10b} / +; r4-GAL4 / UAS-GFP*
	w; UAS-RFP / +; r4-GAL4 / UAS-wild type Akt
	w; UAS-Toll^{10b} / +; r4-GAL4 / UAS-wild type Akt
4G	*w; + / +; r4-GAL4, UAS-Toll^{10b}/ UAS-X (X = various transgenes, as indicated)*

Table S1. Full genotypes of flies for each data point. Related to Experimental Procedures and Figures 1-4.

SUPPLEMENTAL EXPERIMENTAL PROCEDURES

Drosophila stocks used in this study

The following stocks obtained from the Bloomington *Drosophila* Stock Center (Bloomington, IN, NIH P40OD018537) were used in this study: UAS-InR^{A1325D} (#8263), UAS-Dp110^{CAAX} (#25908), UAS-RFP (#30556), UAS-GFP (2nd (#1521) and 3rd (#1522) chromosome insertions), UAS-Dif^{RNAi} (#30513), UAS-Pdk1^{RNAi} (#27725), hsFLP22 (#8862), Act5c>Cd2>Gal4 (#4780), tGPH (#8163), r4-GAL4 (#33832). Other flies used were: UAS-Toll^{10b} (Hu et al., 2004), *rictor*$^{\Delta 2}$ (Hietakangas and Cohen, 2007), UAS-Akt1.HA (wild type) and UAS-myrAkt (Verdu et al., 1999), and *Pdk1*$^{\Delta 33}$ (Cheng et al., 2011).

Construction of UAS-Akt^{T342D} and UAS-Pdk1 transgenic flies

For UAS-Akt^{T342D} and UAS-Pdk1 transgenes, full-length cDNAs (Akt: clone SD10374 and Pdk1: clone LD22131 (836 aa isoform), *Drosophila* Genomics Resource Center, Bloomington, IN, NIH 2P40OD010949) were amplified with gene-specific primers engineered to contain carboxy-terminal HA (Akt) or myc (Pdk1) tags. PCR products were cloned into pENTR (Invitrogen), and phosphorylation site mutations (including phospho-mimicking T342D) were introduced by site-directed mutagenesis (Q5 kit, New England Biolabs). Primer sequences used for cloning and site-directed mutagenesis are listed at the end of this section. Gateway cloning (Invitrogen) was used to generate pUAST-Akt^{T342D}.HA and pUAST-Pdk1.myc. Transgene constructs were injected into *Drosophila* embryos at Rainbow Transgenics (Camarillo, CA). Standard genetics was used to map and generate balanced transgenic lines.

Construction of a myc-tagged *Pdk1* allele

CRISPR/Cas9 was used to insert a myc epitope tag at the 3' end of the final coding exon of *Pdk1*, which is common to all splice variants. The Fly CRISPR Optimal Target Finder (Gratz et al., 2014) was used to identify a CRISPR target site located just upstream of the *Pdk1* stop codon (Figure S4A,B) and with only one predicted off-target site on the X chromosome (*Pdk1* is on chromosome 3). Oligos encoding the *Pdk1* CRISPR-targeting RNA were annealed and ligated into the BbsI site of pU6-BbsI-chiRNA, and PCR was used to create the template for in vitro transcription of the gRNA using the MEGAscript T7 kit (Ambion). The donor template for homology-directed repair consisted of a 200 nucleotide ssDNA oligo with 79 and 81 nt left and right homology arms flanking the myc epitope tag coding sequence, which was engineered immediately 5' of the *Pdk1* stop codon. The PAM sequence of the gRNA binding site in the donor template was mutated, and two additional stop codons in the two alternate reading frames were added downstream of the original stop codon (Figure S4B). Oligonucleotide sequences are listed at the end of this section. See Supplementary Figure 4 for further details.

The gRNA and ssDNA donor template (synthesized as a PAGE-Purified Ultramer by Integrated DNA Technologies, Coralville, IA) were analyzed by separation on a 10% TBE-Urea gel (Bio-Rad) and found to be intact and full-length. The gRNA and ssDNA donor template were injected into *nos-Cas9*/*CyO* embryos at Rainbow Transgenics (Camarillo, CA). Standard fly genetics was used to balance putative insertion lines and to remove *nos-Cas9*. Out of 120 injected embryos, 35 F0 flies were fertile, and eight F1 lines were established for each fertile F0 line. The F1 lines were screened by Western blotting for the myc epitope tag, and four F0 lines bearing the insertion were identified. PCR-based genotyping and sequencing were carried out on each of these four lines to validate insertions (Figure S4C). Insertion lines were further tested by Western blotting to assess: 1) dose-dependent increase in myc-tag signal in *Pdk1*^{myc}/+ compared with *Pdk1*^{myc}/*Pdk1*^{myc} animals (Figure S4D) and 2) elimination of myc-tag signal in fat body lysates from larvae expressing UAS-Pdk1^{RNAi} under control of r4-GAL4 (Figure S4E). We noted no fertility, viability or growth defects in flies heterozygous or homozygous for *Pdk1*^{myc} alleles compared with wild type, suggesting that the myc insertion has negligible effect on Pdk1 function. We also noted that both fat body and whole animal-lysates show that the major Pdk1 splice variant expressed in larvae is the 755 aa (85.6 kDa) form rather than the 539 or 836 aa forms (61 or 94.1 kDa). The *Pdk1*^{myc1} allele was used for protein expression experiments in Figure 3.

Whole-mount Immunocytochemistry

Fat bodies bearing clones of cells expressing UAS-transgenes, generated using the FLP; Act5c>Cd2>GAL4 system (Pignoni and Zipursky, 1997), were dissected from mid-third instar larvae. Fat bodies were fixed in 4% paraformaldehyde for 20 min, blocked in 10% normal donkey and goat sera (Jackson ImmunoResearch) in PBS with 0.1% Triton X-100 (10% ND/GS-T) for 30 min, then incubated overnight at 4°C with mouse anti-Cd2 and rabbit anti-GFP (to detect tGPH) or rabbit anti-phosphoSer505-Akt, diluted in 1% ND/GS-T. The next day, fat bodies were washed in 1% ND/GS-T, incubated with goat anti-rabbit Alexa488 and donkey anti-mouse Cy3 secondary antibodies, diluted in 1% ND/GS-T, for 2 h at room temperature, counterstained with DAPI (Sigma-Aldrich), and mounted on slides in Fluoromount G (Electron Microscopy Sciences).

Western blot analysis

Whole larvae or adult flies (2/sample) or dissected fat bodies (6-10 pooled/sample) were sonicated in 2% SDS and 60 mM Tris-HCl, pH 6.8 with protease inhibitors (Roche Diagnostics) and phosphatase inhibitors. Equal amounts of protein (10-30 µg, measured by BCA assay, Pierce) were separated by SDS-PAGE, proteins were transferred to nitrocellulose, blocked in 3% milk in TBS with 0.1% Tween-20 (TBS-T), and blotted overnight at 4˚C with primary antibodies diluted in 1% milk in TBS-T. Following washes, blots were incubated with secondary antibodies in 1% milk in TBS-T, washed again, incubated with ECL (Pierce), and exposed to film. For phospho-specific antibodies, nitrocellulose membranes were blocked in 3% BSA in TBS-T, and blotted overnight at 4˚C with primary antibodies diluted in 1% BSA in TBS-T. Wash steps, secondary antibody incubation, and detection were performed as described above.

Antibodies used in this study, dilutions, catalog numbers and sources

Immunocytochemistry:
rat anti-mouse Cd2, 1:8000 (MCA154GA, AbD Serotec)
rabbit anti-GFP, 1:8000 (A11122, Invitrogen)
donkey anti-mouse Cy3, 1:300 (715-165-150, Jackson ImmunoResearch)
goat anti-rabbit Alexa488, 1:300 (111-545-003, Jackson ImmunoResearch)

Western blotting:
rabbit anti-phosphoSer505-Akt, 1:1000 (same dilution for immunocytochemistry, 4054, Cell Signaling Technology)
rabbit anti-mouse Akt, 1:1000 (9272, Cell Signaling Technology)
mouse anti-myc tag, 1:5000 (2276, Cell Signaling Technology)
rabbit anti-human Histone H3, 1:5000 (4499, Cell Signaling Technology)
goat anti-rabbit HRP, 1:10,000 (111-035-003, Jackson ImmunoResearch)
goat anti-mouse HRP, 1:10,000 (115-035-003, Jackson ImmunoResearch)

Quantitative RT-PCR

Total RNA was isolated from mid-third instar larval fat bodies (n = 6-8 pooled/sample) using the Reliaprep Tissue RNA Miniprep kit (Promega). Reverse transcription was performed on 1-2 µg total RNA using the ProtoScript First Strand cDNA Synthesis kit (New England Biolabs). Quantitative PCR reactions were performed on 20 ng cDNA, in triplicate, on a Bio-Rad CFX Connect Real-Time PCR Detection System using SYBR Select Master Mix (Life Technologies). Relative amounts of transcripts were calculated using the comparative C_T method using *Rp49* as a reference gene (Schmittgen and Livak, 2008). Gene-specific primer sequences are listed on the next page.

Primers and oligonucleotides used in this study (all listed 5' to 3')

Cloning primers, UAS-Akt-HA and UAS-Pdk1-myc:

Akt-F	CACCATGTCAATAAACACAACTTTCGACC
Akt-HA-R	CTAGGCGTAATCGGGCACATCGTAGGGGTACATTTGCATCGATGCGAGACTTGTGG
Pdk1-F	CACCATGCCGGCTATGGCCAAGGAGAAAGCATCAGC
Pdk1-myc-R	TTACAGATCCTCCTCGGAGATCAGCTTCTGCTCCATCTTAGACGCCGTCTTCTTGCTAGGTGACG

Site-directed mutagenesis primers to generate Akt point mutants:

T342D-F	AGACTTCTGCGGTACACCGGAATAC
T342D-R	TTAGTTGTGCGGCCGTAGGTGAT
T342A-F	AGCTTTCTGCGGTACACCGGAATAC
T342A-R	TTAGTTGTGCGGCCGTAGGTGAT
S505A-F	TTCGCCTACCAAGGAGACATGGCC
S505A-R	CTGGGGGAAAAGCGGCTCTTCGGC
S505D-F	CCAGGGAGACATGGCCTCCACG
S505D-R	TAGTCGAACTGCGGGAAAAGCGG

Primers for synthesis of *Pdk1* gRNA:

Pdk1-myc-gRNA-F	CACCGACGTCACCTAGCAAGAAGA
Pdk1-myc-gRNA-R	AAACTCTTCTTGCTAGGTGACGTC
T7-sgR-F	TTAATACGACTCACTATAGGACGTCACCTAGCAAGAAGAGTTTTAGAGCTAGAAATAG
T7-sgR-R	AAAAGCACCGACTCGGTGCC

ssDNA homology-directed repair template:

AGCTTCGACGGCGTCTGACAACCGGACATTGGGTAGCACCAGAACGGGGACGTCACCTAGCAAGAAGACAACGTCTAAGA
TGGAGCAGAAGCTGATCTCCGAGGAGGATCTGTAAATAACGTAGTCCTATTTATAGCAATGTGAAATTAATTTAGTTGAA
ATTTAGTGCAAACGAAGCGATGGCGTAGAAGAGGGCGGGA

Genotyping: *Pdk1^{myc}* allele generated with CRISPR/Cas9:

Pdk1-myc-F1	ATGCTATCCACTGGTCGGAAG
Pdk1-myc-R1	CCTAAGCACAATACAAATCGGA
Pdk1-myc-R2	CTCGGAGATCAGCTTCT

Primers for Q-PCR:

InR-F	GCCAATTCAATAGCGGGATAC
InR-R	CTCGCATAGAACGGATTCACC
chico-F	CGTCGGAAAAGCTTGCTAAG
chico-R	GTCCCGTATCATTCAAGTGTC
PI3K92E-F	TACTGGACTACGCCTATCCAG
PI3K92E-R	CTTTCCAGGTACGATTCGTGC
Pten-F	GCCACAGAAAATGCAAAGCCA
Pten-R	GCCGGAAACTGGTATTGATGGT
Pdk1-F	CGCGACTCATCTATATCGATC
Pdk1-R	GTCAGACGCCGTCGAAGCTTG
Akt-F	ATGACGCCATCTGAACAGAC
Akt-R	CTTCTCGCGACACAAAATAACC
rictor-F	CCGTAAAAGGCATCGAAGTAC
rictor-R	GTGGTAGCTTCTCGTAGCTGTA
Tor-F	ATTTGGGTGAGGGAGAGCATC
Tor-R	CTGCTCCAAAACATTGTCGC
Phlpp-F	ACTTGCAGTTGCAGGTGGAC
Phlpp-R	ATCGACTAGGCTCCAATGGC
Drs-F	ACCAAGCTCCGTGAGAACCT
Drs-R	CTTGCACACACGACGACAG
Rp49-F	GACGCTTCAAGGGACAGTATCTG
Rp49-R	AAACGCGGTTCTGCATGA

SUPPLEMENTAL REFERENCES

Andjelkovic, M., Jones, P.F., Grossniklaus, U., Cron, P., Schier, A.F., Dick, M., Bilbe, G., and Hemmings, B.A. (1995). Developmental regulation of expression and activity of multiple forms of the Drosophila RAC protein kinase. J. Biol. Chem. *270*, 4066–4075.

Cheng, L., Locke, C., and Davis, G.W. (2011). S6 kinase localizes to the presynaptic active zone and functions with PDK1 to control synapse development. J. Cell Biol. *194*, 921–935.

Gratz, S.J., Ukken, F.P., Rubinstein, C.D., Thiede, G., Donohue, L.K., Cummings, A.M., and O'Connor-Giles, K.M. (2014). Highly Specific and Efficient CRISPR/Cas9-Catalyzed Homology-Directed Repair in Drosophila. Genetics *196*, 961–971.

Hietakangas, V., and Cohen, S.M. (2007). Re-evaluating AKT regulation: role of TOR complex 2 in tissue growth. Genes Dev. *21*, 632–637.

Hu, X., Yagi, Y., Tanji, T., Zhou, S., and Ip, Y.T. (2004). Multimerization and interaction of Toll and Spätzle in Drosophila. Proc. Natl. Acad. Sci. U.S.a. *101*, 9369–9374.

Pignoni, F., and Zipursky, S.L. (1997). Induction of Drosophila eye development by decapentaplegic. Development *124*, 271–278.

Schmittgen, T.D., and Livak, K.J. (2008). Analyzing real-time PCR data by the comparative C(T) method. Nat Protoc *3*, 1101–1108.

Verdu, J., Buratovich, M.A., Wilder, E.L., and Birnbaum, M.J. (1999). Cell-autonomous regulation of cell and organ growth in Drosophila by Akt/PKB. Nat. Cell Biol. *1*, 500–506.